*Geophys. J. Int.* (2009) **000**, 1–**??**

# Saturation and time dependence of geodynamo models

M. Schrinner[1,3⋆], D. Schmitt[1], R. Cameron[1] and P. Hoyng[2]
[1] *Max-Planck-Institut für Sonnensystemforschung, 37191 Katlenburg-Lindau, Germany*
[2] *SRON Netherlands Institute for Space Research, 3584 CA Utrecht, The Netherlands*
[3] *Ecole Normale Supérieur, LRA Département de Physique, 75005 Paris, France*



Accepted Received

**SUMMARY**
In this study we address the question under which conditions a saturated velocity field stemming from geodynamo simulations leads to an exponential growth of the magnetic field in a corresponding kinematic calculation. We perform global self-consistent geodynamo simulations and calculate the evolution of a kinematically advanced tracer field. The self-consistent velocity field enters the induction equation in each time step, but the tracer field does not contribute to the Lorentz force. This experiment has been performed by Cattaneo & Tobias (2009) and is closely related to the test field method by Schrinner et al. (2005, 2007). We find two dynamo regimes in which the tracer field either grows exponentially or approaches a state aligned with the actual self-consistent magnetic field after an initial transition period. Both regimes can be distinguished by the Rossby number and coincide with the dipolar and multipolar dynamo regimes identified by Christensen & Aubert (2006). Dipolar dynamos with low Rossby number are kinematically stable whereas the tracer field grows exponentially in the multipolar dynamo regime. This difference in the saturation process for dynamos in both regimes comes along with differences in their time variability. Within our sample of 20 models, solely kinematically unstable dynamos show dipole reversals and large excursions. The complicated time behaviour of these dynamos presumably relates to the alternating growth of several competing dynamo modes. On the other hand, dynamos in the low Rossby number regime exhibit a rather simple time dependence and their saturation merely results in a fluctuation of the fundamental dynamo mode about its critical state.

**Key words:** Dynamo: theories and simulations; Earth's core; geomagnetic field; magnetohydrodynamics.

## 1 INTRODUCTION

The time variability of cosmic magnetic fields has always been an argument in favour of hydromagnetic dynamo action. Its understanding is crucial for insights in the interior dynamics of stars and planets. The time dependence of convective dynamos is attributable to a non-stationary buoyancy flux as well as to a time dependent equilibration of the magnetic field. The latter is subject of the study presented here.

How do dynamos saturate and in particular in which way is the saturation reflected in their time dependence? In a general description, the infinite growth of a magnetic field due to an appropriate motion of a conducting fluid is inhibited owing to the backreaction of the Lorentz force on the flow; the resulting changes in the flow cause a reduction of dynamo action. Flows which are influenced by the Lorentz force in this way are called saturated. Nevertheless, Cattaneo & Tobias (2009) as well as Tilgner & Brandenburg (2008) demonstrate that saturated flows may lead to exponential growth of the magnetic field in a corresponding kinematic calculation. Despite the fact that the magnetic field is saturated in the full non-linear system, it can grow in a kinematic treatment, because both associated linearized stability problems are different. The flows taken from a saturated dynamo simulation and then used in a kinematic calculation need only quench the growth of the particular magnetic field found in the nonlinear problem and can in principle allow others to grow. As Tilgner & Brandenburg (2008) have pointed out there is at least one example, the benchmark dynamo case 1 (Christensen et al. 2001), where the field taken from a saturated dynamo is also kinematically stable.

In this study, we show that there is in fact a whole class of saturated, chaotic, time-dependent dynamos for which the corresponding kinematic dynamo is stable. In order to assess kinematic stability – in the sense explained above – we solve the MHD-equations for a Boussinesq fluid in a rotating spherical shell. At the same time we evolve a second passive tracer field using the induction equation. While the tracer field experiences the self-consistent velocity field at each time step it does not contribute to the Lorentz force. This method has been used by Cattaneo & Tobias (2009) for box simulations and a shell model and is closely related to the test-field

⋆ E-mail: martin@schrinner.eu

method to determine mean-field coefficients (Schrinner et al. 2005, 2007).

Within a sample of 20 models, we identify two distinct dynamo regimes dependent on a modified Rossby number (Christensen & Aubert 2006) in which the tracer field either grows exponentially or reaches a state aligned with the actual self-consistent magnetic field after an initial transition period. Moreover, differences in the kinematic stability of the dynamos are linked to differences in their time variability: Exclusively kinematically unstable dynamos in the high Rossby number regime show polarity reversals of the axial dipole field. We attribute the complicated time behaviour of these models to an alternating growth of many competing dynamo modes. On the other hand, the eigenvalue computation suggests that dynamos with low Rossby number are dominated by only one fundamental mode which is repeatedly quenched and rebuilt. All other modes in this case are clearly subcritical. In this sense, dynamo models in the low Rossby number regime, i.e. fast rotators, exhibit a simple time dependence and their time-variability consists of fluctuations about their critical state.

## 2 DYNAMO CALCULATIONS

We consider an electrically conducting Boussinesq fluid in a rotating spherical shell and solve the MHD-equations as given by Olson et al. (1999) and described in detail by Christensen & Wicht (2007). In addition, we compute the evolution of a passive tracer field with the help of a second induction equation

$$\partial \boldsymbol{B}_{\rm Tr}/\partial t = \boldsymbol{\nabla} \times (\boldsymbol{u} \times \boldsymbol{B}_{\rm Tr}) + 1/Pm \nabla^2 \boldsymbol{B}_{\rm Tr} \qquad (1)$$

While the tracer field, $\boldsymbol{B}_{\rm Tr}$, experiences the self-consistent velocity field $\boldsymbol{u}$ in each time step, it does not contribute to the Lorentz force. Hence it does not act on the velocity field and is "passive" in this sense. The initial conditions for the tracer field have been chosen arbitrarily with the help of a random number generator. Moreover, for models 10–15, we added some random noise to the tracer field in each time step. This enables us to perturb the tracer field permanently and prevents it from becoming aligned with the actual, self-consistent field. In these simulations, we advance the tracer field for at least 10 magnetic diffusion times in order to test for kinematic stability.

According to the scaling we used, the equations are governed by four parameters. These are the Ekman number $E = \nu/\Omega D^2$, the (modified) Rayleigh number $Ra = \alpha_T g_0 \Delta T D/\nu\Omega$, the Prandtl number $Pr = \nu/\kappa$ and the magnetic Prandtl number $Pm = \nu/\eta$. In these expressions, $\nu$ denotes the kinematic viscosity, $\Omega$ the rotation rate, $D$ the shell width, $\alpha_T$ the thermal expansion coefficient, $g_0$ is the gravitational acceleration at the outer boundary, $\Delta T$ stands for the temperature difference between the inner and outer spherical boundaries, $\kappa$ is the thermal and $\eta = 1/\mu\sigma$ the magnetic diffusivity with the magnetic permeability $\mu$ and the electrical conductivity $\sigma$. All four parameters have been varied to build up a sample of 20 dynamo models, see Table 1.

Output parameters used here in order to interpret the results are the magnetic Reynolds number, $Rm = UD/\eta$, the Elsasser number, $\Lambda = B^2/\varrho\mu\eta\Omega$, and the Rossby number, $Ro = U/D\Omega$. In these expressions, $U$ and $B$ denote rms-values of the velocity and the magnetic field inside the shell, respectively, and $\rho$ is the density. Furthermore, we adopt the definition of a local Rossby number proposed by Christensen & Aubert (2006),

$$Ro_l = Ro \cdot \frac{\bar{l}}{\pi} \qquad (2)$$

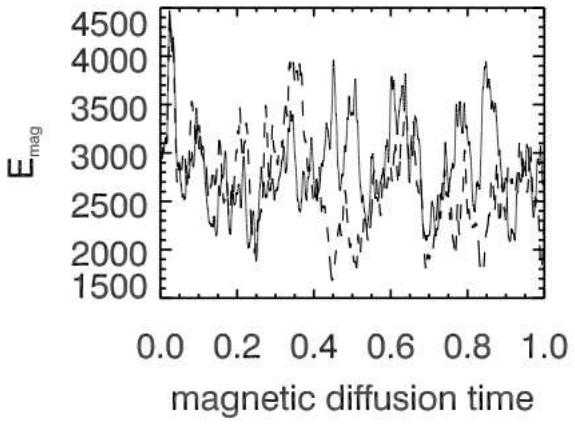


**Figure 1.** Magnetic energy densities for two computational runs of model 2. Both runs have been started from very similar initial conditions which differ only by a small deflection (dashed line) of the magnetic dipole axis. Nevertheless, both models evolve differently which demonstrates the chaotic character of these dynamos.

Here, $\bar{l}/\pi$ is the mean half wavelength of the flow and $\bar{l}$ is the mean harmonic degree derived from the kinetic energy spectrum,

$$\bar{l} = \sum_l l \frac{< \boldsymbol{u}_l \cdot \boldsymbol{u}_l >}{< \boldsymbol{u} \cdot \boldsymbol{u} >} \qquad (3)$$

The brackets in Eq. (3) denote an average over time and radii, $\boldsymbol{u}_l$ stands for the velocity component of harmonic degree $l$.

## 3 RESULTS

Within our 20 examples (see Table 1) we find 5 dynamos which are kinematically unstable and 14 which are kinematically stable. One example (model 15) belongs to both classes; although in general unstable, the tracer field does not grow within certain periods of several magnetic diffusion times. Note that all dynamos considered here operate in the so called strong field regime, i.e. the Elsasser number is of order unity or larger. The equatorial symmetry is broken for most of the kinematically stable and all unstable models. Except for model 1, the quasi-steady benchmark dynamo (Christensen et al. 2001), all models exhibit highly time-dependent or even chaotic behaviour. This is demonstrated in Fig. 1 for model 2, the next simplest example to the benchmark dynamo. This dynamo appears to be chaotic, and as an experiment we performed two simulations starting from almost identical initial conditions (the difference between two initial conditions is a small deflection of the magnetic dipole axis in the second run). The evolution from both initial conditions is shown in Fig. 1 where the magnetic energy densities can be seen to diverge rapidly with time.

The regimes of kinematically stable and unstable dynamos can be clearly distinguished by the modified Rossby number (see Table 1), $Ro_l$. Models with low Rossby number are kinematically stable whereas the tracer field grows exponentially for dynamos in the high Rossby number regime. The transition between both regimes occurs at $Ro_l \approx 0.12$. There are two further properties related to both regimes which deserve mentioning. All dynamos we found to be kinematically stable are dipolar and do not show any polar-

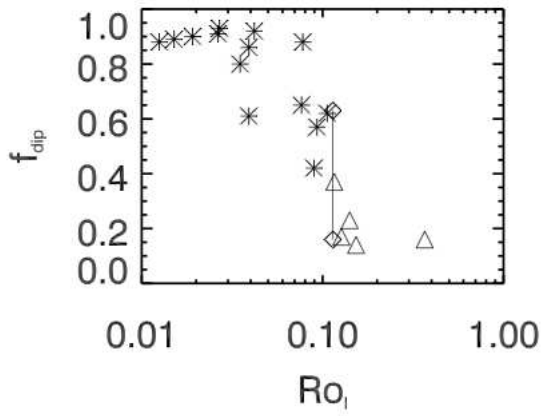


**Figure 2.** Relative dipole field strength $f_{\rm dip}$ versus local Rossby number $Ro_l$. Stars denote non-reversing dynamos which are kinematically stable, whereas triangles represent dynamos which do reverse and are kinematically unstable. Both regimes coincide with the dipolar and multipolar dynamo regimes identified by Christensen and Aubert (2006). There is one example (diamonds), model 15, which undergoes a transition between both regimes. Note that this example has a considerably lower relative dipole field strength in its second state.

ity reversals, while dynamos in the second regime are multipolar and do reverse. This is also illustrated in Fig. 2. Here, the relative dipole field strength, $f_{\rm dip}$, on the outer shell boundary is plotted versus the modified Rossby number, $Ro_l$; $f_{\rm dip}$ is defined as the time-average ratio of the dipole field strength to the field strength in harmonic degrees 1 to 12. Both regimes visible in Fig. 2 coincide with those identified earlier by Christensen & Aubert (2006). Figure 3 compares the magnetic energy densities of the tracer field for a kinematically stable (model 8) and a kinematically unstable dynamo (model 19), varying with time. While the tracer field grows rapidly after an initial transient phase in the latter case, it reaches

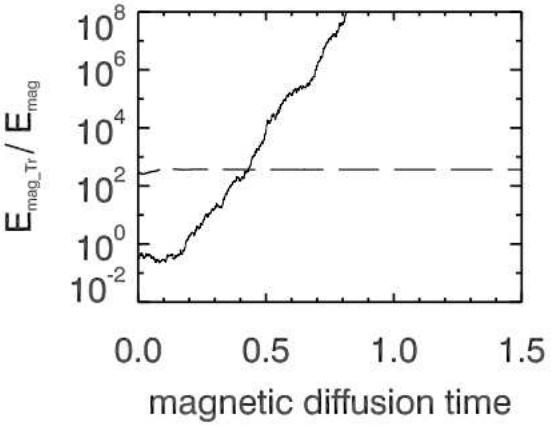


**Figure 3.** Ratio of the magnetic energy densities for the tracer field, $E_{\rm mag_{Tr}}$, and the actual magnetic field, $E_{\rm mag}$, versus time for model 8 (dashed line) and model 19 (solid line).

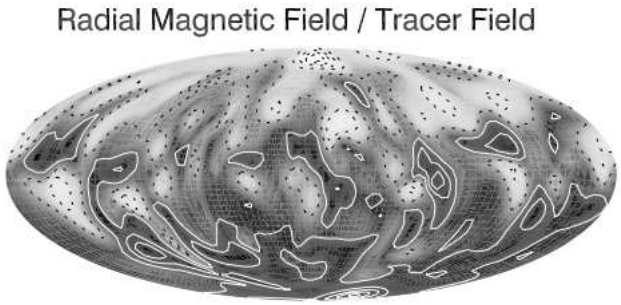


**Figure 4.** Snapshot of the radial component of the actual magnetic field and the tracer field for model 8 taken some time after an initial transition period at $r = 0.62 r_o$ where $r_o$ is the outer shell radius. Note that the tracer field is completely aligned with the actual magnetic field. Both components are normalised due to their maxima and minima. Therefore the greyscale coding varies from -1, white, to +1, black, and the contour lines correspond to $\pm 0.1, \pm 0.3, \pm 0.5, \pm 0.7, \pm 0.9$. Following contour plots are presented in the same style.

a state aligned with the actual field if the dynamo is kinematically stable. Then, the energy density of the tracer field normalised with the energy density of the actual self-consistent field approaches a constant level which depends only on the initial conditions. This is also confirmed by looking at the corresponding field configurations. Figure 4 displays the radial component of the tracer field for model 8, which differs from the actual field only by an overall scale factor. Therefore, only one contour plot is given. On the other hand, although they have similar spatial scales, both field components are clearly not aligned but very different for model 19 (see Fig. 5).

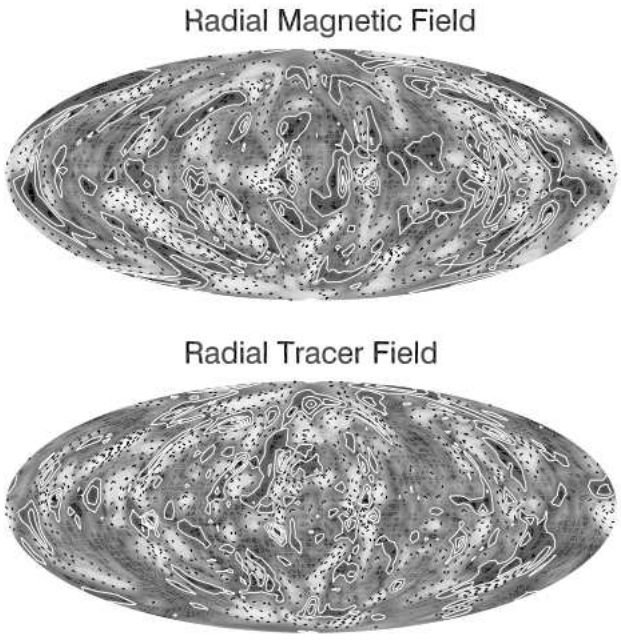


**Figure 5.** Snapshots of the radial component of the actual magnetic field (top) and the tracer field (bottom) for model 19 at $r = 0.62 r_o$. Contour lines: see figure 4.

**Table 1.** Overview of the runs considered, ordered with respect to their modified Rossby number. All kinematically unstable models exhibit dipole reversals whereas all kinematically stable models do not.

| Model | $E$ | $Ra$ | $Pm$ | $Pr$ | $Ro$ | mean $l$ | $Ro_l$ | $f_{\rm dip}$ | $Rm$ | $\Lambda$ |
|---|---|---|---|---|---|---|---|---|---|---|
| | | | | | Kinematically stable models | | | | | |
| model 1 | $1\times10^{-3}$ | 100 | 5 | 1 | 0.0079 | 5 | 0.013 | 0.88 | 39 | 6.3 |
| model 2 | $1\times10^{-4}$ | 334 | 2 | 1 | 0.0043 | 11 | 0.015 | 0.89 | 86 | 1.0 |
| model 3 | $3\times10^{-4}$ | 195 | 3 | 1 | 0.0067 | 9 | 0.019 | 0.92 | 67 | 0.6 |
| model 4 | $3\times10^{-4}$ | 243 | 2 | 1 | 0.0085 | 9 | 0.024 | 0.93 | 56 | 1.7 |
| model 5 | $3\times10^{-4}$ | 285 | 2 | 1 | 0.0092 | 9 | 0.026 | 0.91 | 61 | 2.2 |
| model 6 | $3\times10^{-4}$ | 375 | 3 | 1 | 0.0110 | 10 | 0.035 | 0.80 | 110 | 5.7 |
| model 7 | $3\times10^{-4}$ | 330 | 9 | 3 | 0.0094 | 13 | 0.039 | 0.63 | 283 | 11.9 |
| model 8 | $3\times10^{-4}$ | 330 | 3 | 3 | 0.0094 | 13 | 0.039 | 0.86 | 95 | 2.7 |
| model 9 | $3\times10^{-4}$ | 375 | 1.5 | 1 | 0.0120 | 11 | 0.042 | 0.92 | 60 | 2.0 |
| model 10 | $3\times10^{-4}$ | 630 | 3 | 1 | 0.0200 | 12 | 0.076 | 0.65 | 200 | 6.8 |
| model 11 | $1\times10^{-4}$ | 1117 | 1.5 | 1 | 0.0128 | 19 | 0.078 | 0.88 | 129 | 2.3 |
| model 12 | $1\times10^{-3}$ | 400 | 10 | 1 | 0.0352 | 8 | 0.090 | 0.42 | 352 | 20.0 |
| model 13 | $3\times10^{-4}$ | 810 | 5 | 1 | 0.0244 | 12 | 0.093 | 0.57 | 406 | 18.0 |
| model 14 | $3\times10^{-4}$ | 750 | 3 | 1 | 0.0257 | 13 | 0.106 | 0.62 | 257 | 5.5 |
| | | | | | Kinematically unstable models | | | | | |
| model 15 | $3\times10^{-4}$ | 810 | 3 | 1 | 0.0276 | 13 | 0.114 | 0.61 (0.16) | 276 | 4.7 |
| model 16 | $1\times10^{-3}$ | 450 | 10 | 1 | 0.0406 | 9 | 0.116 | 0.37 | 406 | 19.0 |
| model 17 | $1\times10^{-3}$ | 500 | 10 | 1 | 0.0442 | 9 | 0.127 | 0.17 | 442 | 10.5 |
| model 18 | $3\times10^{-4}$ | 1050 | 3 | 1 | 0.0340 | 13 | 0.141 | 0.23 | 341 | 2.2 |
| model 19 | $3\times10^{-4}$ | 1250 | 3 | 0.3 | 0.0479 | 10 | 0.153 | 0.14 | 479 | 7 |
| model 20 | $3\times10^{-4}$ | 2970 | 1 | 0.3 | 0.1154 | 10 | 0.367 | 0.16 | 385 | 0.4 |

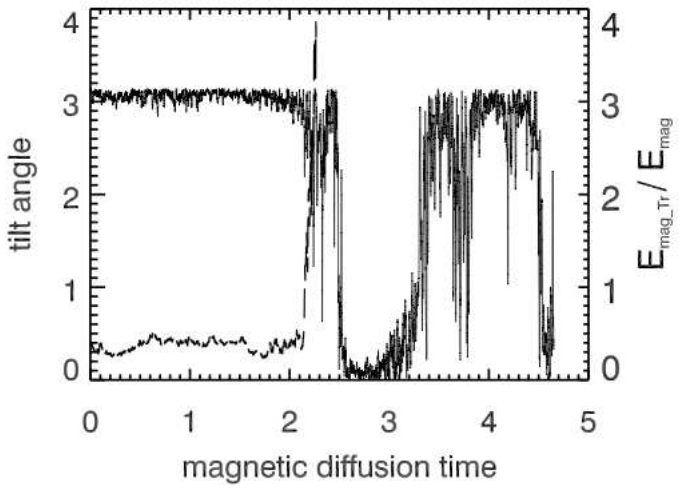


**Figure 6.** Tilt angle of the dipole axis for model 15 as a function of time (solid line) and magnetic energy density of the tracer field normalised by the magnetic energy density of the actual field, $E_{\rm mag_{Tr}}/E_{\rm mag}$ (dashed line which runs out of the figure at roughly 2.3 magnetic diffusion times). As soon as the dynamo reverses it becomes kinematically unstable.

Model 15 is in general kinematically unstable but also exhibits periods of several magnetic diffusion times in which the tracer field stays stable. According to its local Rossby number, $Ro_l = 0.114$, it is located close to the boundry between both dynamo regimes and undergoes transitions from one to the other.

We could detect transitions from a kinematically stable to an unstable state (see Fig. 6) and vice versa. As long as the tracer field remains stable, the tilt angle of the dipole axis fluctuates about the actual polarity state. However, when the tracer field becomes unstable, also the polarity of the dipole field starts to reverse. This coincidence is observed for transitions in both directions, i.e. the tilt angle of the dipole axis also stabilises when model 15 becomes intermittently stable. While the magnetic field is quite dipolar with $f_{\rm dip} = 0.61$ for periods in which the polarity and the tracer field are stable the relative dipole field strength decreases drastically to $f_{\rm dip} = 0.16$ otherwise. The strong connection of field morphology, time dependence and saturation is not only present separately in several models but manifests itself in the time variation of a single dynamo model, too.

## 4 DISCUSSION

The existence of kinematically unstable dynamos was expected (Cattaneo & Tobias 2009; Tilgner & Brandenburg 2008). The finding of a class of kinematically stable but yet time-dependent or even chaotic dynamos, however, needs some further explanation. The lack of growing modes for these models already suggests that almost all field configurations for the tracer field are decaying, except the one aligned with the actual, self-consistent field. But this component of the tracer field is quenched by the saturated velocity field. Thus, the tracer field follows the actual field with time, apart from a different, arbitrary amplitude due to the linearity of the induction equation.

This interpretation is confirmed by looking at the spectrum of the time and azimuthally averaged dynamo operator $D$,

$$D\boldsymbol{b}^i = \lambda^i \boldsymbol{b}^i \tag{4}$$

**Figure 7.** Radial components of the thirst three dipolar eigenmodes $\boldsymbol{b}^i, i = 1 \ldots 3$ of the time averaged dynamo operator for model 2. The corresponding eigenvalues are $\lambda_1 = -3.87$, $\lambda_2 = -34.83$ and $\lambda_3 = -42.45$ in units of $\eta/D^2$. Note the huge drop in decay rates after $\lambda_1$.

with eigenmodes $\boldsymbol{b}^i$ and eigenvalues $\lambda^i$. In this, the operator $D$ is defined as

$$D\boldsymbol{b} = \boldsymbol{\nabla} \times (\bar{\boldsymbol{u}} \times \boldsymbol{b} + \boldsymbol{\alpha} \cdot \boldsymbol{b} - \boldsymbol{\beta}\, \boldsymbol{\nabla}\boldsymbol{b} - \eta \boldsymbol{\nabla} \times \boldsymbol{b}) \tag{5}$$

Note that $D$, also known as mean-field dynamo operator (Krause & Rädler 1980), contains the mean velocity field $\bar{\boldsymbol{u}}$ as well as the so called mean-field coefficients $\boldsymbol{\alpha}$ and $\boldsymbol{\beta}$, which are tensors of second and third rank, respectively. As noted by Hoyng (2009), these quantities appear inevitably as a consequence of averaging. They depend on the velocity field and the magnetic diffusivity of the considered dynamo model only and have been determined with the help of the test field method (Schrinner et al. 2005, 2007). A detailed discussion on the applicability of mean-field concepts to direct numerical simulations of rotating magnetoconvection and a (quasi-)stationary dynamo is provided by Schrinner et al. (2007). A similar discussion for time dependent dynamos is not given here but will be subject of a forthcoming paper. A recent review on the test-field method and its applications has been given by Brandenburg (2009).

Eigenvalues and eigenmodes of $D$ have been computed as reported by Schrinner et al. (2009) for model 2. In Fig. 7 the radial components of the first three (dipolar) eigenmodes, $\boldsymbol{b}^i$, are displayed. All modes decay exponentially; this had to be expected for kinematically stable dynamos (see also the discussion in Hoyng 2009). However, the decay rates are given here in units of $\eta/D^2$, in which the molecular diffusivity $\eta$ is about 30 times smaller than the turbulent one inferred from components of $\boldsymbol{\beta}$. Thus, $1/|\lambda_1| \approx 1/4$ is much larger than one effective diffusion time and the first, fundamental, eigenmode is indeed close to its critical state. Due to a noticable gap in decay rates after the fundamental mode, $|\lambda_1| \ll |\lambda_2|$, this is not equally true for the subsequent eigenmodes. They are much more diffusive, thus leaving the fundamental mode as the preferred eigenstate of the dynamo. Hence, the time dependence of model 2 may be understood in parts as a fluctuation of the fundamental mode about its critical state.

The dominance of the first eigenstate is also revealed by a decomposition of the actual, time-dependent magnetic field of model 2 in a set of eigenmodes $\boldsymbol{b}^i$ of $D$,

$$\boldsymbol{B}(\boldsymbol{r}, t) = \sum_i a^i(t) \boldsymbol{b}^i(\boldsymbol{r}) \tag{6}$$

The time-dependent and in general complex mode coefficients $a^i(t)$ have been computed as

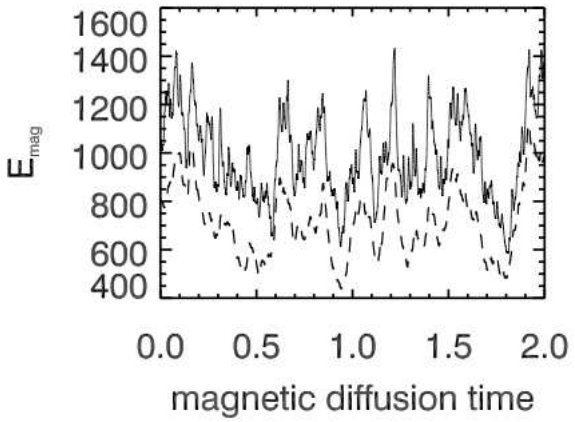


**Figure 8.** Axisymmetric magnetic energy density (solid line) and energy contribution of the first, fundamental eigenmode (dashed line) varying with time. The fundamental eigenmode $a^1(t)\boldsymbol{b}^1(\boldsymbol{r})$ already contributes 75% up to 85% to the total amount and its time variability reflects much of the time dependence of the axisymmetric magnetic field.

$$a^i(t) = \int_V \hat{\boldsymbol{j}}^i(\boldsymbol{r}) \cdot \boldsymbol{A}(\boldsymbol{r}, t)\, \mathrm{d}^3\boldsymbol{r} \tag{7}$$

in which $\hat{\boldsymbol{j}}^i$ denotes the adjoint of the current $\boldsymbol{j}^i = \boldsymbol{\nabla} \times \boldsymbol{b}^i$, and $\boldsymbol{A}$ is the vector potential of the actual, time-dependent field, $\boldsymbol{B} = \boldsymbol{\nabla} \times \boldsymbol{A}$. The integration is carried out over the whole fluid domain $V$. For a derivation of Eq. (7) we refer to Hoyng (2009) and Schrinner et al. (2009).

In Fig. 8 the energy contribution of the fundamental eigenmode $a^1(t)\boldsymbol{b}^1(\boldsymbol{r})$ is compared with the total axisymmetric magnetic energy density. The fundamental eigenmode contributes at least 75% up to 85% to the total amount, revealing again its permanent dominance throughout the simulation.

The equilibration process for model 2 has been studied earlier by Olson et al. (1999), too. They found that in regions with high magnetic energy density, the Lorentz force simply reduces locally the flow velocity without changing the overall pattern of convection. They investigated possible changes in the velocity, if the magnetic field and thus the Lorentz force is arbitrarily reduced at some instant in time and then recovers towards its equilibration value. The kinematic effects relevant for dynamo action identified by them, an $\alpha$-effect from helicity in the columnar convection and an anti-$\omega$ effect from the mean azimuthal flow, were present in the same proportions close and far from equilibrium conditions of the magnetic field. Their finding is supported by the study presented here. Saturation may reduce the amplitudes of $\alpha$ and thus the growth rates of the eigenstates of the related dynamo operator, but does not change their relative order. Therefore, the preferred eigenstate stays the same throughout the simulation. This is clear as there is a large gap between the growth rate of the fundamental eigenmode of the time-averaged dynamo operator $D$ and all other eigenmodes, as mentioned above.

So far we only analysed model 2 in detail. Here the velocity field is nearly symmetric with respect to the equatorial plane and the magnetic field belongs to the dipolar family. Contributions of quadrupolar type are not present. In a more complicated example with broken equatorial symmetry, we expect the fundamental

quadrupolar mode to be excited. Although its growth rate will be smaller than the one for the fundamental dipolar mode and probably subcritical, it is typically of the same order. In such a case a clear dominance of only one fundamental dipolar mode can no longer be deduced from the spectrum of the time-averaged dynamo operator $D$, and a second, quadrupolar mode may become important.

For the models in the high Rossby number regime the findings of Cattaneo & Tobias (2009) apply. These models act kinematically as dynamos and the dynamo operator $D$ possesses in general growing eigenmodes. A kinematic treatment of these dynamos does not reveal their actual time dependence. However, the results presented here suggest that the regime of dipolar dynamos identified by Christensen & Aubert (2006) is kinematically stable. For these models, the quenching of any magnetic field is fully captured in the velocity field and a kinematic treatment may indeed reproduce their actual time-dependence. Models of this dynamical regime are applicable to planetary dynamos and probably also to dynamos of fast rotating stars (Christensen et al. 2009a), thus covering a large range of magnetic Reynolds numbers. Hence, an attempt to explain the kinematic stability of these models due to a magnetic Reynolds number which is close to its critical value fails. We emphasise again that the transition between both regimes is governed by the local Rossby number $Ro_l$ and not by $Rm$, as can be already seen from Table 1. In the low Rossby number regime, the rotational constraint leads to columnar structured flows, dipolar magnetic fields and finally to a rather simple time dependence, although these models operate in general far away from the dynamo threshold at $Rm_c \approx 40$.

Dipolar dynamo models which show occasionally reversals are located close to the regime boundary in Fig. 2, with $Ro_l \leq 0.12$. They resemble the geodynamo in many respects and are therefore of particular interest. Explaining polarity reversals of an otherwise predominantly dipolar field, Olson & Christensen (2006) suggest that the geodynamo crosses the boundary towards the multipolar dynamo regime from time to time. With the help of scaling laws derived from numerical models, they indeed succeed in predicting a local Rossby number of $Ro_l \approx 0.09$ for the Earth's core. Adopting this viewpoint we link the occurence of geomagnetic reversals to a change in the saturation process. The quenching of a previously dipolar field may result in the preference of different, higher order modes if inertia gains importance in comparison to the coriolis force, and the dynamo undergoes an excursion into the kinematically unstable regime. Subsequently the dipole field is built up again, but it may have either polarity. A computation of eigenmodes and a mode decomposition similar to (6) for model 15 seems to be a promising approach to confirm this picture. Note that from the viewpoint we take here, the existence of dipolar, stable periods for model 15 demands more explanation than the fact that it reverses.

However, whether inertia is indeed as important for the geodynamo as it is for present dynamo models is under debate (e.g. Sreenivasan & Jones 2006). In fact, the assumption of $Ro_l \approx 0.09$ for the Earth's core leads to a characteristic length scale of only a few hundred meters, on which the magnetic field would be highly diffusive (Christensen et al. 2009b).

## 5 CONCLUSIONS

Fast rotating dynamos, characterised by a low Rossby number, are kinematically stable. Within this regime, a saturated velocity field taken from dynamo simulations does not lead to exponential growth of the magnetic field in a corresponding kinematic calculation. Hence, saturation may be understood as a quality of the velocity field, only. For these dynamos, saturation results in the unchanged preference of a fundamental eigenstate, whereas different eigenmodes may supersede each other if inertia gains importance. This difference in the saturation process involves differences in the morphology of the magnetic field and its time dependence. Kinematically stable dynamos are dipolar and exhibit a rather simple time variability, which may be interpreted as the fluctuation of the fundamental mode about its critical state. Kinematically unstable dynamos are much more complicated. The alternating growth of various modes leads to a multipolar field morphology and polarity reversals of the dipole field appear as a natural consequence.

## ACKNOWLEDGMENTS

We thank Ulrich Christensen and Johannes Wicht for many interesting discussions and support.

## REFERENCES

Brandenburg, A., 2009. Advances in theory and simulations of large-scale dynamos, *Space Sci. Rev.*, **144**, 87–104.

Cattaneo, F. & Tobias, S.M., 2009. Dynamo properties of the turbulent velocity field of a saturated dynamo, *J. Fluid Mech.*, **621**, 205–214.

Christensen, U.R., Aubert, J., Cardin, P., Dormy, E., Gibbons, S., Glatzmaier, G.A., Grote, E., Honkura, Y., Jones, C., Kono, M., Matsushima, M., Sakuraba, A., Takahashi, F., Tilgner, A., Wicht, J. & Zhang, K., 2001. A numerical dynamo benchmark, *Phys. Earth. Planet. Inter.*, **128**, 25–34.

Christensen, U.R. & Aubert, J., 2006. Scaling properties of convection-driven dynamos in rotating spherical shells and application to planetary magnetic fields, *Geophys. J. Int.*, **166**, 97–114.

Christensen, U.R. & Wicht, J., 2007. Numerical dynamo simulations, in *Treatise on Geophysics, Vol. 8*, pp. 245–282, ed. Schubert G., Elsevier, Amsterdam.

Christensen, U.R., Holzwarth, V. & Reiners, A., 2009a. Energy flux determines magnetic field strength of planets and stars, *Nature*, **457**, 167–169.

Christensen, U.R., Schmitt, D. & Rempel, M., 2009b. Planetary dynamos from a solar perspective, *Space Sci. Rev.*, **144**, 105–126.

Hoyng, P., 2009. Statistical dynamo theory: Mode excitation, *Phys. Rev. E*, **79**, 046320, 1–13.

Krause, F. & Rädler, K.-H., 1980. Mean-Field Magnetohydrodynamics and Dynamo Theory, Pergamon Press, Oxford.

Olson, P. & Christensen, U.R., 2006. Dipole moment scaling for convection driven planetary dynamos, *Earth Planet. Sci. Lett.*, **250**, 561–571.

Olson, P., Christensen, U.R. & Glatzmaier, G.A., 1999. Numerical modeling of the geodynamo: Mechanisms of field generation and equilibration, *J. Geophys. Res.*, **104**, 10383–10404.

Schrinner, M., Rädler, K.-H., Schmitt, D., Rheinhardt, M. & Christensen, U.R., 2005. Mean-field view on rotating magnetoconvection and a geodynamo model, *Astron. Nachr.*, **326**, 245–249.

Schrinner, M., Rädler, K.-H., Schmitt, D., Rheinhardt, M. & Christensen, U.R., 2007. Mean-field concept and direct numerical simulations of rotating magnetoconvection and the geodynamo, *Geophys. Astrophys. Fluid Dynam.*, **101**, 81–116.

Schrinner, M., Schmitt, D., Jiang, J. & Hoyng, P., 2009. A new method for computing the eigenfunctions and their adjoints of the dynamo operator, *Mon. Not. R. Astron. Soc.*, submitted.

Sreenivasan, B. & Jones, C.A., 2006. The role of inertia in the evolution of spherical dynamos, *Geophys. J. Int.*, **164**, 467–476.

Tilgner, A. & Brandenburg, A., 2008. A growing dynamo from a saturated Roberts flow dynamo, *Mon. Not. R. Astron. Soc.*, **391**, 1477–1481.